CHINESE OPTICS LETTERS

Vol. 21, No. 3 | March 2023

High-stability 4H-SiC avalanche photodiodes for UV detection at high temperatures

Xingye Zhou (周幸叶), Yuanjie Lü (吕元杰)*, Hongyu Guo (郭红雨), Xubo Song (宋旭波), Yuangang Wang (王元刚), Shixiong Liang (梁士雄), Aimin Bu (卜爱民), and Zhihong Feng (冯志红)**

National Key Laboratory of ASIC, Hebei Semiconductor Research Institute, Shijiazhuang 050051, China

*Corresponding author: yuanjielv@163.com

**Corresponding author: ga917vv@163.com

Received June 21, 2022 | Accepted September 30, 2022 | Posted Online October 28, 2022

In this work, high-stability 4H-SiC avalanche photodiodes (APDs) for ultraviolet (UV) detection at high temperatures are fabricated and investigated. With the temperature increasing from room temperature to 150°C, a very small temperature coefficient of 7.4 mV/°C is achieved for the avalanche breakdown voltage of devices. For the first time, the stability of 4H-SiC APDs is verified based on an accelerated aging test with harsh stress conditions. Three different stress conditions are selected with the temperatures and reverse currents of 175°C/100 μA, 200°C/100 μA, and 200°C/500 μA, respectively. The results show that our 4H-SiC APD exhibits robust high-temperature performance and can even endure more than 120 hours at the harsh aging condition of 200°C/500 μA, which indicates that 4H-SiC APDs are very stable and reliable for applications at high temperatures.

Keywords: silicon carbide; photodiode; UV detector; high temperature; avalanche; Geiger mode.

DOI: 10.3788/COL202321.032502

1. Introduction

Due to the high-quality and chemically stable material, wide bandgap semiconductor avalanche photodiodes (APDs) based on silicon carbide (SiC) have advantages of being photosensitive, visible-blind, reliable, small, and easily integrated, which makes them powerful competitors for ultraviolet (UV) detectors in plenty of applications, such as corona detection, astronomical research, UV communication, and missile plume detection[1–5]. In the past few years, with the improvement of crystal material growth and device fabrication technology, 4H-SiC APDs have achieved great advancements with high gain, high quantum efficiency (QE), low dark current, and even excellent Geiger-mode single-photon-detection performance[6–13]. Related arrays based on 4H-SiC APDs have also been demonstrated for UV imaging in the future[14–18]. However, most of the reported research work has been focused on 4H-SiC APDs at low temperatures. For such critical applications as flame detetion in gas turbines and UV detection for space exploration, high-stability UV detectors at high temperatures are in great demand. The temperature-dependent performance of 4H-SiC APD-based UV detectors has been analyzed by few research groups in the world[19–21]. The stability and reliability of 4H-SiC APDs with harsh stress conditions have not yet been reported.

In this Letter, high-stability 4H-SiC APDs at high temperatures are fabricated and investigated for UV detections. Based on the variable-temperature I–V test, junction temperature test, and accelerated aging test, the stability of 4H-SiC APDs is extensively analyzed and verified. With the temperature increasing from room temperature to 150°C, a stable avalanche breakdown voltage is obtained with a very small temperature coefficient of 7.4 mV/°C for 4H-SiC APD devices. In addition, the high-temperature stability of our 4H-SiC APDs was verified with a high junction temperature of ~270°C by using an infrared microscope. Finally, for the first time (to the best of our knowledge), the stability of 4H-SiC APDs is further proved based on an accelerated aging test under harsh stress conditions. Three different stress conditions are selected with the temperatures and reverse currents of 175°C/100 μA, 200°C/100 μA, and 200°C/500 μA, respectively. Our 4H-SiC APDs can endure more than 120 h, even at the aging condition of 200°C/500 μA. The results in this work indicate that 4H-SiC APDs are very stable and reliable in harsh environments at high temperatures.

2. Device Design and Fabrication

First, the device structure of 4H-SiC APDs is carefully designed, which determines the performance under dark current, avalanche breakdown voltage, QE, etc. As shown in Fig. 1(a), a separate absorption charge multiplication (SACM) epilayer structure is used for our 4H-SiC APDs in this work. From

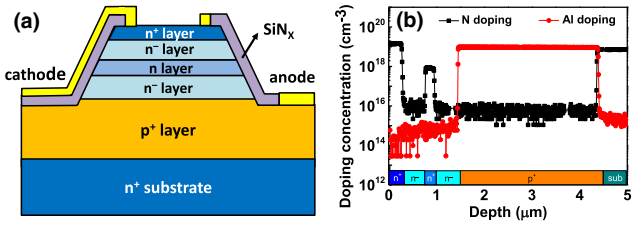

Fig. 1. Device structure of 4H-SiC APDs. (a) Schematic cross-sectional structure; (b) doping concentration profile of epilayers obtained by SIMS.

bottom to top, the wafer is composed of a p^+ layer with a thickness of 3 μm and a doping concentration of $N_a = 1 \times 10^{19}$ cm^{-3}, a 0.5 μm-thick n^- multiplication layer with a doping concentration of $N_d = 1 \times 10^{15}$ cm^{-3}, an n charge layer with a thickness of 0.2 μm and a doping concentration of $N_d = 1 \times 10^{18}$ cm^{-3}, a 0.5 μm-thick n^- absorption layer with a doping concentration of $N_d = 1 \times 10^{15}$ cm^{-3}, and a 0.3 μm-thick n^+ contact layer with a doping concentration of $N_d = 1 \times 10^{19}$ cm^{-3}. By chemical vapor deposition (CVD), the epimaterial was grown on an n^+ 4H-SiC substrate according to the optimized epistructure. During the growth process of the 4H-SiC epilayers, nitrogen donors and aluminum acceptors were used for n-type and p-type *in situ* doping, respectively. The doping concentration profile of epilayers is obtained by secondary ion mass spectroscopy (SIMS), as illustrated in Fig. 1(b). It should be noted that the low doping concentration is limited to 1×10^{16} cm^{-3} by the measurement system of SIMS. It can be seen that the doping concentration profile of the grown crystal material matches that of the designed structure.

Device fabrication was based on an optimized manufacturing process, and the detailed fabrication process can be referred to in Ref. [22]. For isolation and passivation, a SiN_x layer with a thickness of 500 nm was deposited by dual-frequency plasma-enhanced chemical vapor deposition (PECVD). The SiN_x in the active area of 4H-SiC APD was removed to open an optical window. The active area diameter of the fabricated 4H-SiC APDs is 150 μm. Finally, the chip was attached into a TO46 package for the accelerated aging test.

3. Results and Discussion

The room-temperature performance of 4H-SiC APDs was first investigated. As shown in Fig. 2(a), the dark current and photocurrent at $\lambda = 280$ nm as well as the multiplication gain M of 4H-SiC APDs were characterized as a function of the reverse voltage. The photo image of the fabricated 4H-SiC APD is shown in the inset of Fig. 2(a). It is shown that the dark current maintains at a very low level of about 10 pA until the avalanche breakdown happens near 163 V. With the definition of a unity gain at the reverse bias voltage of $V_r = 10$ V, a high avalanche multiplication gain of $M > 10^6$ is calculated for our 4H-SiC APDs. The spectral responsivity of 4H-SiC APDs at the unity gain was measured based on a monochromator, and a silicon UV photodetector was used to calibrate the power of a xenon lamp light source.

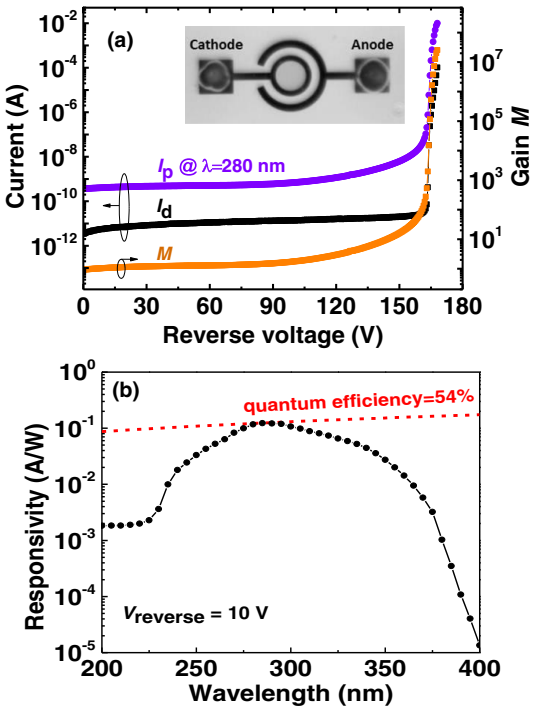

Fig. 2. Characteristics of 4H-SiC APDs at room temperature. (a) *I-V* and *I-M* curves; (b) spectral responsivity. Here, the photo image of the fabricated 4H-SiC APD is shown in the inset of Fig. 2(a).

As shown in Fig. 2(b), a peak responsivity of 0.124 A/W at the wavelength of 285 nm is obtained, corresponding to the maximum external QE of 54%.

In order to investigate the high-temperature device performances, the I–V characteristics of our 4H-SiC APDs were measured, with the temperatures ranging from room temperature to 150°C. The dark currents as a function of reverse voltage near the breakdown voltage (V_b) are provided in Fig. 3(a), and it is shown that the breakdown voltage shifts positively when the temperature increases. The result suggests that hard avalanche breakdown happens in our devices, which is expected for high-gain APDs. In order to evaluate the V_b shift more clearly, the dependence of V_b shift on the temperature is illustrated in Fig. 3(b), and here V_b is defined as the reverse voltage at which a multiplication gain is 1000. It can be seen clearly from Fig. 3(b) that the avalanche breakdown voltage shifts positively and linearly with the temperature increase. This is because the impact ionization coefficient decreases at high temperatures[22], and a higher reverse voltage is desired to create a stronger electric field for the avalanche effect. For practical usage, a small temperature coefficient is expected for the avalanche breakdown voltage of APDs. With the optimized epitaxial structure, our 4H-SiC APDs exhibit a stable avalanche breakdown voltage with a small temperature coefficient of $C_T = 7.4$ mV/K. As is known, the dark current, breakdown voltage, gain, and temperature coefficient of V_b are determined by the epitaxial structure, which has to be carefully designed for a trade-off between the device performance parameters. The comparison results of different APDs are shown in Table 1, and it can be seen that a very small

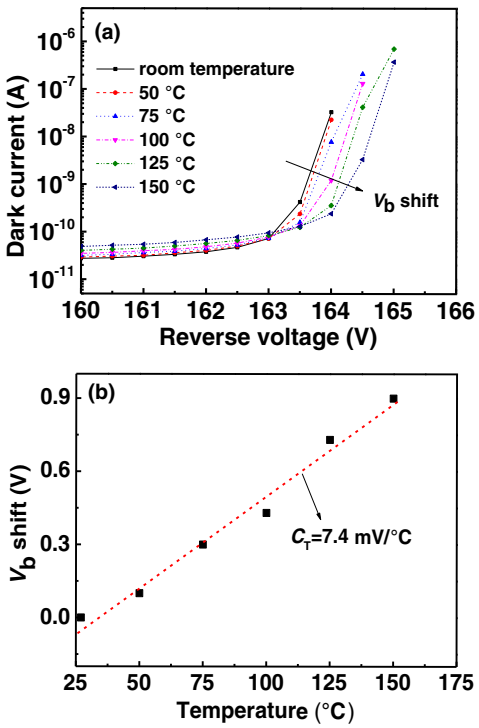

Fig. 3. Performance of 4H-SiC APDs at different temperatures. (a) Dark currents near the breakdown voltage; (b) breakdown voltage shift as a function of temperature.

temperature coefficient of V_b is achieved for our 4H-SiC APD devices. Meanwhile, a small breakdown voltage, low dark current, high gain, and high QE are also obtained. The excellent device performance demonstrates that our 4H-SiC APDs are very stable at high temperatures due to the high-quality epitaxial material, optimized device structure, and fabrication process.

In addition, the high-temperature stability of our 4H-SiC APDs was verified with a high junction temperature, as shown in Fig. 4. The two-dimensional mapping of junction temperature was obtained for our fabricated 4H-SiC APDs based on an infrared microscope, during which the device was stressed with large power consumption and high temperatures. Figures 4(a) and 4(b) provide the junction temperature mapping of 4H-SiC

Table 1. Comparison of Different 4H-SiC APDs.

Parameters	Ref. [19]	Ref. [20]	This Work
V_b (V)	634	186	163
I_{dark}@95% V_b (A/μm^2)	5×10^{-14}	1.7×10^{-17}	1.1×10^{-15}
Gain	2500	$>10^6$	$>10^6$
Maximum QE (%)	45%@290 nm	53%@290 nm	54%@285 nm
C_T of V_b (mV/°C)	110	14	7.4

Note: I_{dark} denotes the dark current, QE is the quantum efficiency, and C_T means the temperature coefficient. Here, V_b, I_{dark}@95% V_b, gain, and the maximum QE are the results measured at room temperature.

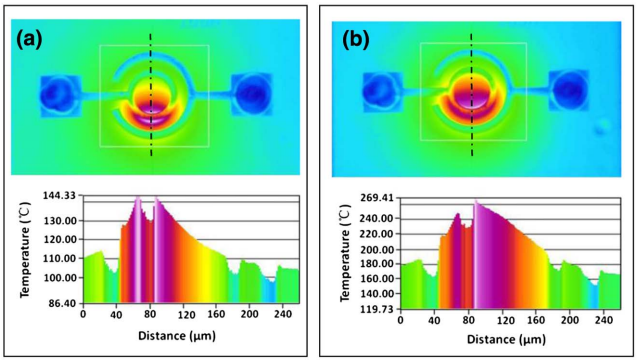

Fig. 4. Two-dimensional mapping of the junction temperature for 4H-SiC APDs with different maximum junction temperatures. (a) 145°C; (b) 270°C.

APD with different maximum junction temperature of 145°C and 270°C, respectively. It should be noted that the distribution of junction temperature is nonuniform for 4H-SiC APDs, which can be explained by the asymmetric carrier lateral drift in the off-orientated 4H-SiC[7,22–25]. The results demonstrate that the fabricated 4H-SiC APD can bear a junction temperature of ~270°C [see Fig. 4(b)], proving the stability of our devices at high temperatures.

Finally, for the first time, an accelerated aging test with harsh stress conditions was performed to further confirm the stability of 4H-SiC APDs in this work. Three different stress conditions are selected with the temperatures and reverse currents of 175°C/100 μA, 200°C/100 μA, and 200°C/500 μA, respectively. The stress condition for 4H-SiC APDs in this work is much harsher than that of the aging test for InGaAs APDs in Ref. [26]. Device failure is defined as a state in which the dark current at a bias of 0.5 V over the avalanche breakdown voltage increases more than 0.01 μA compared with the initial value. A pre-aging test of 24 h at the stress condition of 175°C/100 μA was done to check the bonding of the device sample, and the first 24 h of pre-aging did not result in changes in the dark-current characteristics.

After the pre-aging, a long-time aging test was conducted. The dark-current variation of 4H-SiC APD as a function of accelerated aging time with different stress conditions is shown in Fig. 5. The dark current was measured at room temperature with

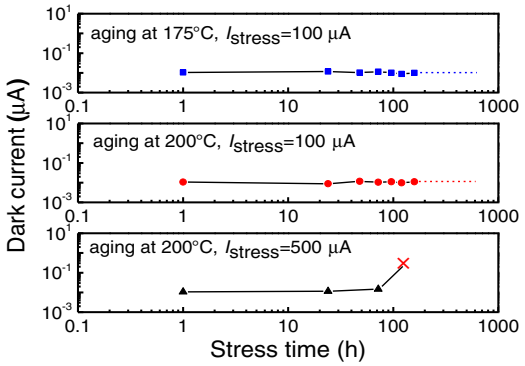

Fig. 5. Dark current of 4H-SiC APD as a function of aging time with different stress conditions. (a) 175°C/100 μA; (b) 200°C/100 μA; (c) 200°C/500 μA.

a reverse bias voltage, where a gain of $M = 1000$ was obtained. It demonstrates that there is almost no degradation in the dark current of 4H-SiC APD after 120 h of aging at the condition of 175°C/100 μA and 200°C/100 μA. With the aim to accelerate the degradation of the device sample, a harsher stress condition with a reverse bias current of 500 μA at the temperature of 200°C was chosen. The fabricated 4H-SiC APD can endure more than 120 h, even at the aging condition of 200°C/500 μA. After 129 h of aging under the harsh condition of 200°C/500 μA, the device sample failed, with hard breakdown. In practical usage, 4H-SiC APDs usually operate with a low-level dark current of a few pico- or nanoamperes. Therefore, our 4H-SiC APDs can actually endure many more hours at 200°C. To our knowledge, this is the first report that verifies the stability of 4H-SiC APDs based on an accelerated aging test. The reliability and lifetime of 4H-SiC APDs will be further investigated based on more device samples in our ongoing work in the future.

4. Conclusion

In conclusion, high-stability 4H-SiC APDs are fabricated and investigated for UV detection at high temperatures. The high-temperature stability of our 4H-SiC APDs was verified based on the variable temperature $I - V$ test, a high junction temperature, and the accelerated aging test under harsh stress conditions. A stable avalanche breakdown voltage with a very small temperature coefficient of 7.4 mV/°C is achieved from room temperature to 150°C. The fabricated 4H-SiC APDs can bear a high junction temperature of ~270°C and can endure more than 120 h at the aging condition of 200°C/500 μA. The results in this work indicate that 4H-SiC APDs have the capability to operate in harsh environment at high temperatures.

Acknowledgement

This work was supported by the National Natural Science Foundation of China (No. 61974134) and the Hebei Province Outstanding Youth Fund (No. F2021516001).

References

1. T. Liu, P. Wang, and H. Zhang, "Performance analysis of non-line-of-sight ultraviolet communication through turbulence channel," Chin. Opt. Lett. **13**, S21501 (2015).
2. X. Guo, L. B. Rowland, G. T. Dunne, J. A. Fronheiser, P. M. Sandvik, A. L. Beck, and J. C. Campbell, "Demonstration of ultraviolet separate absorption and multiplication 4H-SiC avalanche photodiodes," IEEE Photon. Technol. Lett. **18**, 1910 (2006).
3. H.-D. Liu, D. McIntosh, X. Bai, H. Pan, M. Liu, J. C. Campbell, and H. Y. Cha, "4H-SiC PIN recessed-window avalanche photodiode with high quantum efficiency," IEEE Photon. Technol. Lett. **20**, 1551 (2008).
4. H.-D. Liu, X. Zheng, Q. Zhou, X. Bai, D. C. McIntosh, and J. C. Campbell, "Double mesa sidewall silicon carbide avalanche photodiode," IEEE J. Quantum Electron. **45**, 1524 (2009).
5. Q. Zhou, D. McIntosh, H.-D. Liu, and J. C. Campbell, "Proton-implantation-isolated separate absorption charge and multiplication 4H-SiC avalanche photodiodes," IEEE Photon. Technol. Lett. **23**, 299 (2011).
6. A. Vert, S. Soloviev, J. Fronheiser, and P. Sandvik, "Solar-blind 4H-SiC single-photon avalanche diode operating in Geiger mode," IEEE Photon. Technol. Lett. **20**, 1587 (2008).
7. X. Cai, D. Zhou, S. Yang, H. Lu, D. Chen, F. Ren, R. Zhang, and Y. Zheng, "4H-SiC SACM avalanche photodiode with low breakdown voltage and high UV detection efficiency," IEEE Photon. J. **8**, 6805107 (2016).
8. X. Zhou, T. Han, Y. Lv, J. Li, W. Lu, Y. Wang, X. Tan, S. Liang, Z. Feng, and S. Cai, "Large-area 4H-SiC ultraviolet avalanche photodiodes based on variable-temperature reflow technique," IEEE Electron Device Lett. **39**, 1724 (2018).
9. X. Zhou, X. Tan, Y. Wang, X. Song, T. Han, J. Li, W. Lu, G. Gu, S. Liang, Y. Lv, and Z. Feng, "Large-area 4H-SiC avalanche photodiodes with high gain and low dark current for visible-blind ultraviolet detection," Chin. Opt. Lett. **17**, 090401 (2019).
10. X. Bai, H.-D. Liu, D. C. McIntosh, and J. C. Campbell, "High-detectivity and high-single-photon-detection-efficiency 4H-SiC avalanche photodiodes," IEEE J. Quantum Electron. **45**, 300 (2009).
11. J. Hu, X. Xin, X. Li, J. H. Zhao, B. L. VanMil, K.-K. Lew, R. L. Myers-Ward, C. R. Eddy, Jr., and D. K. Gaskill, "4H-SiC visible-blind single-photon avalanche diode for ultraviolet detection at 280 and 350 nm," IEEE Trans. Electron Devices **55**, 1977 (2008).
12. X. Xin, F. Yan, X. Sun, P. Alexandrove, C. M. Stahle, J. Hu, M. Matsumura, X. Li, M. Weiner, and H. J. Zhao, "Demonstration of 4H-SiC UV single photon counting avalanche photodiode," Electron. Lett. **41**, 212 (2005).
13. X. Zhou, X. Tan, Y. Lv, Y. Wang, J. Li, X. Song, S. Liang, Z. Feng, and S. Cai, "Single-photon-counting performance of 4H-SiC avalanche photodiodes with a wide-range incident flux," IEEE Photon. Technol. Lett. **32**, 847 (2020).
14. A. Vert, S. Soloviev, A. Bolotnikov, and P. Sandvik, "Silicon carbide photomultipliers and avalanche photodiode arrays for ultraviolet and solar-blind light detection," in *IEEE Sensors Conference* (2009), p. 1893.
15. F. Yan, C. Qin, J. H. Zhao, M. Bush, G. Olsen, B. K. Ng, J. P. R. David, R. C. Tozer, and M. Weiner, "Demonstration of 4H-SiC avalanche photodiodes linear array," Solid-State Electron. **47**, 241 (2003).
16. L. Li, D. Zhou, H. Lu, W. Liu, X. Mo, F. Ren, D. Chen, R. Wang, G. Li, R. Zhang, and Y. Zheng, "4H-SiC avalanche photodiode linear array operating in Geiger mode," IEEE Photon. J. **9**, 6804207 (2017).
17. X. Zhou, X. Tan, Y. Lv, Y. Wang, J. Li, T. Han, H. Guo, S. Liang, Z.-H. Zhang, Z. Feng, and S. Cai, "8 × 8 4H-SiC ultraviolet avalanche photodiode arrays with high uniformity," IEEE Electron Device Lett. **40**, 1589 (2019).
18. X. Zhou, X. Tan, Y. Lv, Y. Wang, J. Li, S. Liang, Z.-H. Zhang, Z. Feng, and S. Cai, "128-pixel arrays of 4H-SiC UV APD with dual-frequency PECVD SiN_x passivation," Opt. Express **28**, 29245 (2020).
19. H.-Y. Cha, S. Soloviev, S. Zelakiewicz, P. Waldrab, and P. M. Sandvik, "Temperature dependent characteristics of nonreach-through 4H-SiC separate absorption and multiplication APDs for UV detection," Sens. J. **8**, 233 (2008).
20. D. Zhou, F. Liu, H. Lu, D. Chen, F. Ren, R. Zhang, and Y. Zheng, "High-temperature single photon detection performance of 4H-SiC avalanche photodiodes," IEEE Photon. Technol. Lett. **26**, 1136 (2014).
21. S. Yang, D. Zhou, X. Cai, W. Xu, H. Lu, D. Chen, F. Ren, R. Zhang, Y. Zheng, and R. Wang, "Analysis of dark count mechanisms of 4H-SiC ultraviolet avalanche photodiodes working in Geiger mode," IEEE Trans. Electron Devices **64**, 4532 (2017).
22. R. Raghunathan and B. J. Baliga, "Temperature dependence of hole impact ionization coefficients in 4H and 6H-SiC," Solid-State Electron. **43**, 199 (1999).
23. A. Konstantinov and T. Neyer, "Pattern of near-uniform avalanche breakdown in off-oriented 4H SiC," IEEE Trans. Electron Devices **61**, 4153 (2014).
24. K. Mochizuki, N. Kameshiro, H. Matsushima, H. Okino, and R. Yamada, "Uniform luminescence at breakdown in 4H-SiC 4°-off (0001) p–n diodes terminated with an asymmetrically spaced floating-field ring," IEEE J. Electron Devices Soc. **3**, 349 (2015).
25. L. Su, X. Cai, H. Lu, D. Zhou, W. Xu, D. Chen, F. Ren, R. Zhang, Y. Zheng, and G. Li, "Spatial non-uniform hot carrier luminescence from 4H-SiC p-i-n avalanche photodiodes," IEEE Photon. Technol. Lett. **31**, 447 (2019).
26. I. Watanabe, M. Tsuji, M. Hayashi, K. Makita, and K. Taguchi, "Reliability of mesa-structure InAlGaAs-InAlAs superlattice avalanche photodiodes," IEEE Photon. Technol. Lett. **8**, 824 (1996).